Convective Bursts, Downdraft Cooling, and Boundary Layer Recovery in a Sheared Tropical Storm

JOHN MOLINARI

Department of Atmospheric and Environmental Sciences, University at Albany, State University of New York, Albany, New York

JACLYN FRANK

AWS Truepower, Albany, New York

DAVID VOLLARO

Department of Atmospheric and Environmental Sciences, University at Albany, State University of New York, Albany, New York

(Manuscript received 4 May 2012, in final form 9 October 2012)

ABSTRACT

Tropical Storm Edouard (2002) experienced episodic outbreaks of convection downshear within the storm core in the presence of 11–15 m s^{-1} of ambient vertical wind shear. These outbreaks lasted 2–6 h and were followed by long periods with no deep convection. Flights from U.S. Air Force reconnaissance aircraft within the boundary layer were used to investigate the cause of one such oscillation. Low equivalent potential temperature θ_e air filled the boundary layer as convection ceased, creating a 4–6-K deficit in θ_e within the convective region. Soundings within 110 km of the center were supportive of convective downdrafts, with midlevel relative humidity below 15% and large downdraft CAPE. Deep convection ceased within 75 km of the center for more than 8 h. Tangential velocity reached hurricane force locally during the convective outbreak, then became nearly symmetric after convection stopped, arguably as a result of axisymmetrization, and the storm weakened. Nevertheless, the corresponding lack of convective downdrafts during this period allowed surface heat and moisture fluxes to produce substantial increases in boundary layer entropy. A new burst of convection followed. Consistent with recent papers it is argued that tropical cyclone intensification and decay can be understood as a competition between surface heat and moisture fluxes (''fuel'') and low-entropy downdrafts into the boundary layer (''antifuel'').

1. Introduction

The complex role of ambient vertical wind shear on tropical cyclone structure and intensity has become a major topic of research [see literature reviews by Reasor and Eastin (2012) and Nolan and McGauley (2012)]. Tang and Emanuel (2010) noted that the most effective way to weaken a sheared tropical cyclone is to reduce entropy in the eyewall, which directly reduces the work done in the Carnot cycle described by Emanuel (1986). Using theory and an axisymmetric numerical model with parameterized vertical wind shear, Tang and Emanuel (2010, 2012) showed that one means of reducing eyewall moist entropy was the mixing of low entropy air from the environment into the eyewall by eddies, primarily vortex Rossby waves (Montgomery and Kallenbach 1997). Tang and Emanuel (2012) found such mixing to be least effective in weakening the storm at upper levels, but of considerably greater importance at low and middle levels. Riemer and Montgomery (2011) argued that such mixing might be most influential in weak storms with large ambient shear.

Riemer et al. (2010) and Tang and Emanuel (2012) also discussed the reduction of eyewall entropy as a result of the flux of low equivalent potential temperature θ_e air into the boundary layer from downdrafts excited by

Corresponding author address: John Molinari, University at Albany, State University of New York, Atmospheric and Environmental Sciences, ES-225, 1400 Washington Ave., Albany, NY 12222.
E-mail: jmolinari@albany.edu

DOI: 10.1175/MWR-D-12-00135.1

the evaporation of precipitation. Riemer et al. (2010) imposed vertical wind shear on a mature tropical cyclone and found broad regions of negative moist entropy anomalies associated with this process. Previously Barnes et al. (1983), Powell (1990), and Didlake and Houze (2009) reported observational evidence of downdrafts in tropical cyclones. Low-θ_e downdraft air outside the storm core often did not recover its original θ_e before reaching the eyewall, thereby weakening the storm. Riemer et al. (2010) labeled this cold downdraft air ''antifuel,'' as opposed to the fuel of heat and moisture fluxes from the ocean. They found a 4-K reduction in azimuthally averaged eyewall θ_e for 15 m s^{-1} ambient shear, about 4 times that of eddy-induced mixing shown by Cram et al. (2007). Riemer et al. (2010) argued that negative vertical fluxes of θ_e by downdrafts into the boundary layer provide the primary mechanism by which ambient vertical wind shear weakens a mature tropical cyclone.

Most observational studies of downdraft-driven cold pools in tropical cyclones have examined rainbands outside the storm core (Eastin et al. 2012). The simulations of Riemer et al. (2010) showed vortex-scale bands of downdraft cooling spiraling in from outer radii. Eastin et al. (2005) examined updraft and downdraft cores at all radii. They found that convective-scale downdrafts were typically negatively buoyant in rainbands. In the storm core, negatively buoyant downdrafts were most common left of shear, coexisting with positively buoyant convective updrafts. Weakly positively buoyant unsaturated downdrafts existed upshear. This reflects the variety of downdrafts in nature, both convective scale and mesoscale, as was noted by Zipser (1977).

Few observations have been made of moist entropy changes in tropical cyclones in nature with respect to the ambient vertical wind shear. Shelton and Molinari (2009) described the behavior of strongly sheared Hurricane Claudette (2003). This storm deepened to a hurricane, then weakened so quickly that no closed circulation could be found at 850 hPa 12 h later. Shelton and Molinari found a large 6 K km^{-1} gradient in 850-hPa θ_e adjacent to the upshear eyewall just prior to the rapid weakening. Tang and Emanuel (2012) noted that the simple presence of low-θ_e air near the eyewall is insufficient to account for storm weakening. Rather, an irreversible mixing of low entropy air with eyewall air by eddies or by cold downdrafts was needed. Hurricane Claudette displayed extensive cold cloud tops above the low θ_e air upshear (cf. Shelton and Molinari's Figs. 5c and 8a). These clouds could have produced precipitation into this air that initiated weakening via cold downdrafts, consistent with the virtual elimination of inner-core convection that followed. The difficulty with the Shelton and Molinari (2009) study is that no boundary layer data were available to directly measure the impact of cold downdrafts.

Tang and Emanuel (2012) found that in the presence of strong ventilation by vertical wind shear, an oscillatory behavior developed in which convective outbreaks in the core produced temporary deepening, followed by cold downdrafts cutting off convection and subsequent weakening. The current study investigates similar behavior in Tropical Storm (TS) Edouard (2002). The presence of boundary layer data from aircraft reconnaissance will allow us to address the mechanisms by which strong ambient shear produced such an oscillation.

2. Data and methods

This study uses several data sources: lightning data from the National Lightning Detection Network (Cummins and Murphy 2009); ambient vertical wind shear estimates from the European Centre for Medium-Range Weather Forecasts (ECMWF) gridded analyses; wind, pressure, temperature, moisture, and storm center positions from U.S. Air Force reconnaissance aircraft; flight-level vertical velocity from two National Oceanic and Atmospheric Administration (NOAA) P-3 aircraft; dropsondes from the NOAA G-IV and P-3 aircraft; and sea surface temperature (SST) from the NOAA/Advanced Very High Resolution Radiometer (AVHRR). Air Force flight-level data were available at 10-s intervals (approximately 1 km in space), and P-3 data at 1-min intervals (7-km resolution for the flight segments examined). The processing and use of these data sources is described by Molinari and Vollaro (2010). One difference from previous work is that only the first 10 s of data were removed from the two lower-tropospheric dropsondes examined here, rather than 30 s used for upper-tropospheric sondes.

One of the prime concerns with flight-level data in tropical cyclones is instrument wetting, which typically produces an order of 5-K underestimate of θ_e due to evaporation from the temperature sensor (Eastin et al. 2002). This can complicate detection of downdraft air. Eastin et al. (2002) found that 95% of instrument wetting errors occurred in the presence of nonzero cloud water; only rarely did precipitation in unsaturated air (as might occur in the boundary layer) produce such events. Because the current study uses thermodynamic data only from U.S. Air Force boundary layer flights, it is much less likely that instrument wetting will be a problem. Thermodynamic data from two P-3 flights near 850 hPa will not be displayed, because they contained obvious wetting errors at key locations.

The potential for downdrafts to reach the surface will be measured by two variables: downdraft CAPE (DCAPE)

calculated following Emanuel (1994), and the microburst index of Atkins and Wakimoto (1991). This index was developed for ''wet'' microbursts in high-precipitable water midlatitude convection, which are more likely in tropical cyclones than ''dry'' microbursts. The microburst index is simply θ_e at the surface minus the minimum θ_e in the column. Values exceeding 20–30 K (depending upon location and other variables; see Wheeler and Roeder 1996) are required to make surface microbursts possible.

3. Convective fluctuations in Tropical Storm Edouard

a. Observations of convection and moist entropy

Table 1 shows the minimum central pressure and maximum surface wind speed in TS Edouard from the National Hurricane Center best-track data. Also shown are the ambient 850–200-hPa vertical wind shear direction and magnitude and the underlying SST. Table 1 covers the period from 0000 UTC 2 September to 0000 UTC 4 September, during which Edouard followed an anticyclonic loop just east of the Gulf Stream (Frank 2008; also see storm summary at http://www.nhc.noaa.gov/2002edouard.shtml). Ambient shear remained above 10 m s^{-1} throughout the period. The shear direction remained almost constant from the west-northwest. Two-thirds of the shear existed above 500 hPa, with weak mean winds below that level (Frank 2008). Mean SST under the storm fluctuated in a small range. The storm underwent one brief but sharp intensification in which maximum winds increased more than 10 m s^{-1} between 0600 and 1200 UTC 3 September. Ambient vertical wind shear was near a maximum and SST near a minimum at this time. As a result, changes in shear and SST were not a proximate cause of the intensification. The storm weakened in the following 12 h.

Figure 1 shows a sequence of infrared and visible images every 2 h over a 10-h period that encompasses the strong intensification of the storm. The magenta lines in Figs. 1c,e show U.S. Air Force reconnaissance flight tracks that will be discussed later. The impact of the strong ambient vertical wind shear from the west-northwest (Table 1) is evident in Fig. 1 throughout the period. At 0715 UTC 3 September (Fig. 1a), the center of TS Edouard consisted of a low cloud swirl. Deep convection was confined to more than 100 km from the storm center just left of downshear. Nolan (2011) showed that vertical wind shear played the primary role in creating the convective asymmetries in TS Edouard early on 3 September, just prior to Fig. 1a.

During the following 4 h (Figs. 1b,c), the convection shifted inward toward the center. The coldest cloud-top temperatures (below −75°C) occurred at 1015 UTC (between Figs. 1b,c), after which the cloud tops began to warm. Figures 1e,f show visible images. The core convection decayed by 1715 UTC (Fig. 1f), and the storm once again exhibited a low cloud swirl near the center and deep convection downshear left more than 100 km from the center.

TABLE 1. Evolution of the intensity of Tropical Storm Edouard between 0000 UTC 2 Sep and 0000 UTC 4 Sep 2002 in terms of minimum central pressure and maximum surface wind (from the best-track data of the National Hurricane Center). Also shown are ambient shear from ECMWF analyses following Corbosiero and Molinari (2002). The final column shows the mean sea surface temperature averaged over the inner 25 km of radius in the storm. The latter are taken from 4-km AVHRR values, averaged over 8 days ending 21 Aug 2002, prior to the development of Edouard.

	p_{min} (hPa)	$\lvert\mathbf{v}_{max}\rvert$ (m s^{-1})	ECMWF shear (° @ m s^{-1})	Mean SST (°C)
0000 UTC 2 Sep	1011	15.4	286 @ 12.6	29.1
0600 UTC 2 Sep	1007	18.0	289 @ 14.7	29.6
1200 UTC 2 Sep	1007	18.0	300 @ 12.0	29.4
1800 UTC 2 Sep	1005	18.0	281 @ 10.8	29.3
0000 UTC 3 Sep	1003	18.0	289 @ 14.0	29.1
0600 UTC 3 Sep	1003	18.0	296 @ 13.9	29.0
1200 UTC 3 Sep	1002	28.3	294 @ 13.1	29.2
1800 UTC 3 Sep	1004	23.2	292 @ 14.8	29.1
0000 UTC 4 Sep	1005	20.6	305 @ 19.0	29.4

The sequence of events in Fig. 1 occurred multiple times in TS Edouard. Figure 2 shows a radius–time series of cloud-to-ground lightning flash density. Figure 2 shows that strong inner-core outbreaks initiated near 1200 UTC 2 September, 2100 UTC 2 September, 0900 UTC 3 September, and 0200 UTC 4 September. The most intense lightning cores coincided with OLR minima like those in Fig. 1. These outbreaks were striking in that (i) they lasted only 2–6 h, (ii) they were separated by periods of virtually no lightning in the inner 75 km, and (iii) the length of the quiet periods was roughly proportional to the total flash count within the prior convective outbreak. The satellite depiction of the 0900 UTC 3 September event associated with strong intensification was shown in Fig. 1. Earlier convective outbreaks produced less dramatic intensity changes (Table 1).

The vertical lines in Fig. 2 indicate the times of center crossing by U.S. Air Force reconnaissance. Figure 3 shows the tracks of those flights, using the same color code as in Fig. 2, with the order in time represented by red–green–blue. The red flight track corresponds to that shown in Fig. 1c, and the green to Fig. 1e. The tracks are oriented approximately from right to left of the ambient shear vector. These flight legs are the focus of this

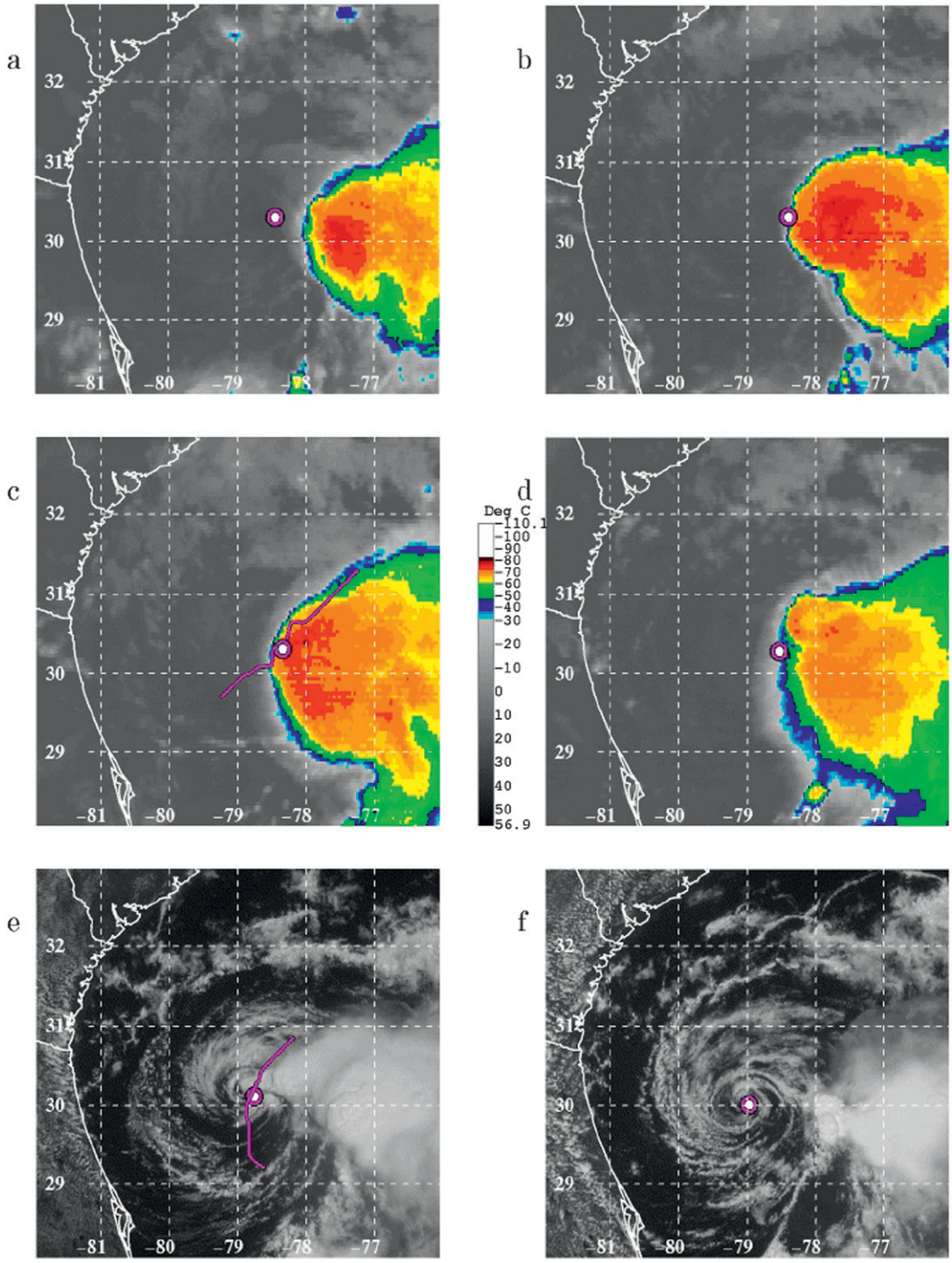

FIG. 1. Infrared satellite images on 3 Sep 2002 at (a) 0715, (b) 0915, (c) 1115, and (d) 1315 UTC. Visible images at (e) 1515 and (f) 1715 UTC. The magenta ring indicates the best-track center position. The magenta lines indicate U.S. Air Force reconnaissance flight tracks that will be discussed with Figs. 3–4.

study because they systematically covered the same quadrants over three consecutive center crossings. Only two full northwest–southeast legs were available; the latter were used only in the calculation of azimuthal means.

The left-of-shear legs in Fig. 3 lie just downwind of the strongest convection (Figs. 1c,e), in the same quadrant where Riemer et al. (2010) showed low entropy air coming closest to the center. The first center crossing

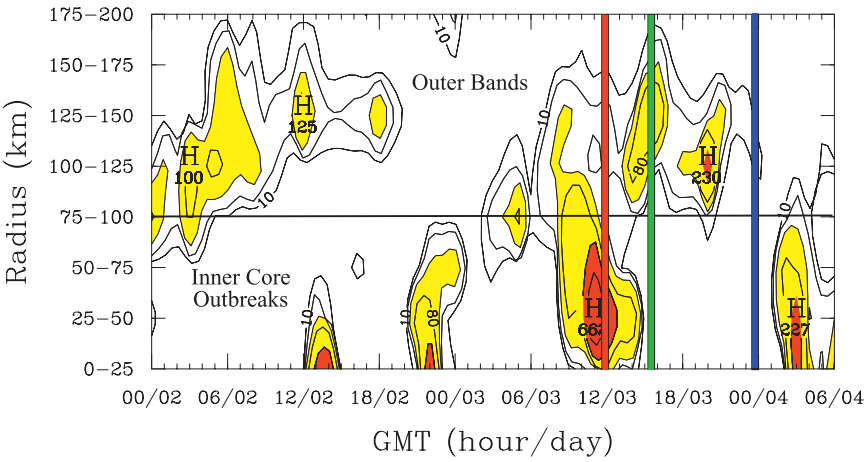

FIG. 2. Radius–time plot of cloud-to-ground flash density per unit time in TS Edouard averaged over 25-km radial bins. Contours increase by factors of 2 beginning with 10 flashes $(10^4\ \text{km}^2)^{-1}\ \text{h}^{-1}$. Yellow and red shading begin at 40 and 160 units, respectively. The red, green, and blue vertical lines represent the times of center crossing of the three U.S. Air Force reconnaissance aircraft tracks shown in Fig. 3.

(red) took place about 2.5 h after the convection began. The second (green) occurred 4 h later, after all core convection had ceased (Fig. 2). The final track (blue) passed through the center after an additional 8 h, at the end of the quiet period and just prior to a new burst of convection. Cross sections of various quantities will be shown for the tracks in Fig. 3. The complex portion of the first flight (black line) was removed for the cross sections; only the straight segments shown in red were used. The flight tracks in Fig. 3 occurred entirely within the boundary layer, ranging from 250- to 500-m elevation (see appendix A, Fig. A1). Appendix A provides evidence that these small elevation changes had little impact on the interpretation of the cross sections in Fig. 4.

Figure 4 contains four panels. The first shows lightning flash density per unit time versus radius summed over two 180° azimuthal segments. One faces northeast (right side of Fig. 4a), and the other southwest, roughly left and right of the ambient vertical wind shear, respectively. The lightning covers a 2-h period from 1100–1259 UTC 3 September, encompassing the first flight in Fig. 3. Figure 4a indicates a strong convective outbreak left of shear that peaked between the 40- and 50-km radii. Much less lightning existed right of shear. By the times of the second and third flights, all lightning in the core had ceased.

Figures 4b,c show the evolution of tangential velocity and θ_e, respectively. During the time of the convective event (red), a hurricane-force wind maximum developed left of shear just inside the radius of the most intense lightning. Right of shear the tangential velocity was mostly below 10 m s^{-1}. After the core convection ceased (green), the tangential velocity began to become more symmetric, suggesting an axisymmetrization of the storm (e.g., Montgomery and Kallenbach 1997; Möller and Montgomery 2000). Wind speed increased right of shear and decreased sharply, with an outward shift in the

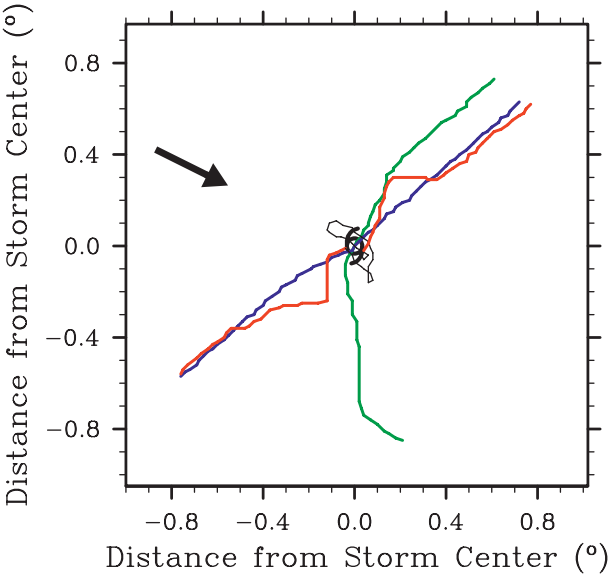

FIG. 3. U.S. Air Force Reserve reconnaissance aircraft tracks on 3 Sep 2002. Only the southwest–northeast segments are shown. Red: 1120–1226 UTC; green: 1529–1603 UTC; and blue: 2326 UTC 3 Sep–0011 UTC 4 Sep. The black line represents part of the first (red) track; only the red portions are used in subsequent radial cross sections. The tracks extend generally from right to left of the ambient vertical wind shear vector shown by the black arrow.

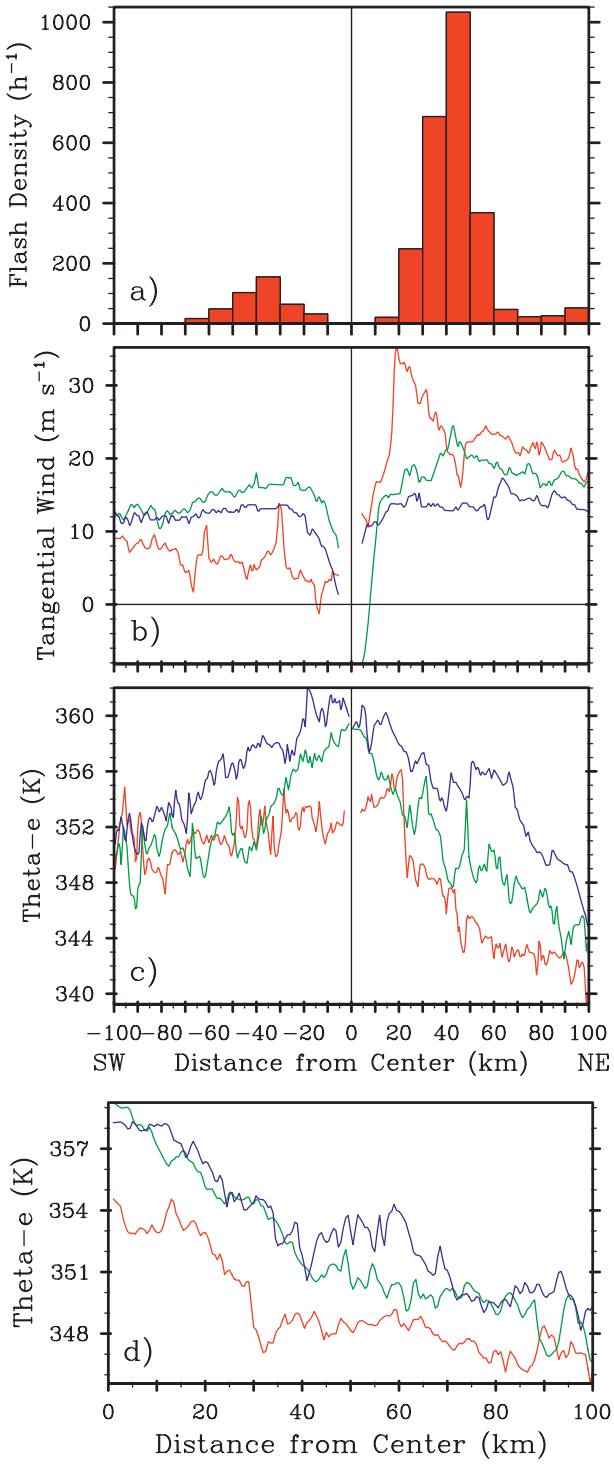

FIG. 4. (a) Radial cross section of lightning density (units as in Fig. 2) for all flashes in the (left side) southwest half of the circulation and (right side) northeast half, in 10-km radial bins, summed over the period from 1100–1259 UTC 3 Sep. (b),(c) Southwest–northeast cross sections from each of the three U.S. Air Force reconnaissance flights displayed in Fig. 3 showing (b) tangential velocity (m s^{-1}) and (c) θ_e (K) with the same color scheme. (d) Azimuthally averaged θ_e (K) using all flight legs between 1121–1342 UTC (red), 1529–1729 UTC (green), and 2326 UTC 3 Sep–0134 UTC 4 Sep (blue).

maximum wind, left of shear. By the final time (blue), the storm exhibited a flat tangential wind speed profile of 12–15 m s^{-1} over a wide region both right and left of shear.

Figure 4c shows cross sections of boundary layer θ_e. At the initial time (red curve), 4–8-K θ_e deficits existed between the convectively active regions left of shear and the inactive regions right of shear, suggesting the presence of convective downdrafts. Over the following 4 h (green), after lightning had ended, the left-of-shear boundary layer began to recover. By the end of the period (blue), θ_e left of shear was nearly equal to that right of shear. Two hours later, a new convective outbreak (Fig. 2) began downshear left.

The time variation of θ_e in Fig. 4c suggests that surface entropy fluxes produced the boundary layer recovery. Appendix B addresses whether this is a reasonable conclusion. Using observed values for surface wind speed, relative humidity, and air–sea temperature differences, it shows that the increase in θ_e in Fig. 4c can be accounted for entirely from surface heat and moisture fluxes. The boundary layer recovery was more dramatic left of shear owing to the low entropy air produced by the earlier convection. The value of θ_e remained large the entire time right of shear, but almost no lightning occurred (Fig. 2), likely due to vertical shear-induced subsidence stabilizing the column (e.g., DeMaria 1996).

Figure 4d shows azimuthally averaged θ_e (using all available radial legs) for three time periods encompassing the three flights. The deficit in θ_e of 4–6 K between the convectively active period and the recovered boundary layer is remarkably similar to the decrease in mean θ_e produced by downdrafts in the simulations by Riemer et al. (2010) using 15 m s^{-1} vertical shear. It is also comparable to θ_e deficits in tropical cyclone cold pools reviewed by Eastin et al. (2012). Lower θ_e during the first flight into TS Edouard extended outward to the 100-km radius (Fig. 4c), consistent with a downshear stationary rainband (Willoughby et al. 1984) described by Riemer et al. (2010).

b. *Evidence for downdrafts*

Powell (1990) and Barnes et al. (1983) argued that low θ_e air can be transported from outer radii to the storm core, where it suppresses convection in the eyewall. This is likely not the case in TS Edouard, because the low θ_e air shown in Fig. 4c is coincident with a maximum in convection, not with a break in the eyewall. As a result, local convective downdrafts were likely responsible for the low θ_e air shown in Figs. 4c,d. The potential for such downdrafts is suggested by Special Sensor Microwave Imager (SSM/I) precipitable water values of only 45 mm upshear throughout 3 September, far below

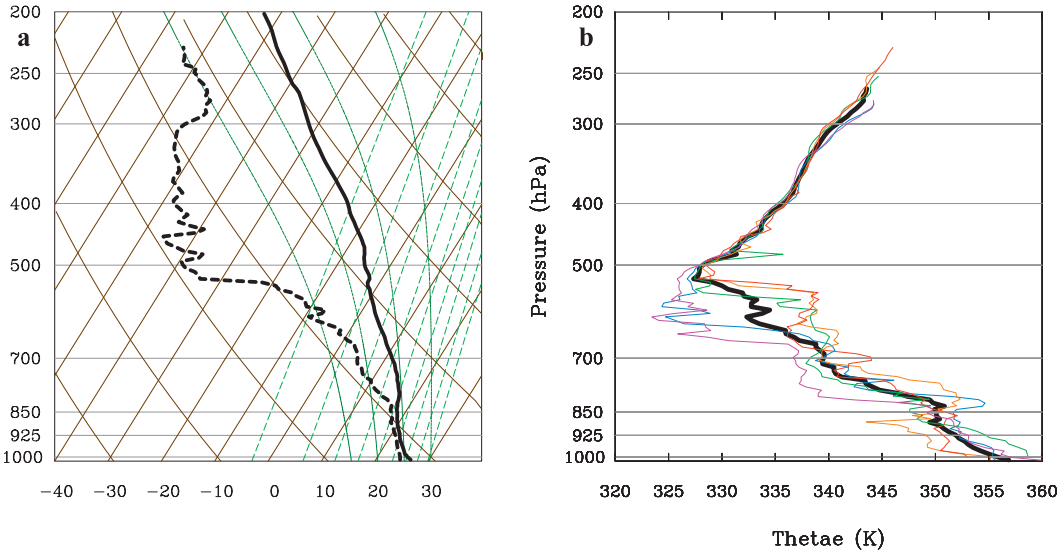

FIG. 5. (a) Mean vertical profiles of temperature and dewpoint from five G-IV sondes released within 110 km of the center between 1803–1816 UTC 3 Sep. (b) Vertical profile of θ_e for each of these sondes. Colors match those of the sonde locations in Fig. 6. The thick black line shows the mean θ_e.

that in the typical tropical cyclone (J. Dunion 2011, personal communication). However, no dropsondes were released by G-IV and P-3 aircraft upshear prior to the convective outbreak centered near 1200 UTC 3 September, and downdraft potential could not be evaluated at that time. Instead, two sets of soundings will be examined from 1800–1900 UTC 3 September. This period falls between the times of the green and blue tracks in Fig. 3.

Figure 5a shows the mean sounding from five G-IV sondes during this period. The locations of these sondes with respect to the storm center are shown by the colored squares in Fig. 6, plotted over the 1845 UTC visible image. All lie within 110 km of the center. Figure 5b shows the vertical profile of θ_e for each of these sondes and for the mean.

Figure 5a shows a near-saturated sounding up to about 850 hPa, but the column dried dramatically above that, with relative humidity below 15% above 500 hPa, even in sondes within 50 km of the storm center. This striking profile arose because extremely dry midtropospheric air upshear over land (not shown) was advected into the storm by vertically sheared flow, at the same time that TS-force winds were enhancing θ_e in the boundary layer. This coexistence of low-θ_e air aloft with high values at the surface was found in sheared pretropical storm disturbances by Smith and Montgomery (2011).

The microburst index of Atkins and Wakimoto (1991) has a mean value of 29 K in the Fig. 5b profiles, sufficient to support microburst downdrafts into the boundary layer if deep convection is excited. The mean θ_e minimum lies near 500 hPa, virtually the same level shown in Atkins and Wakimoto's (1991) downburst events. Maximum DCAPE values (not shown) exceeded 1500 J kg^{-1} in all of these sondes. This exceeds the maximum DCAPE found at any level in three developing and nondeveloping tropical disturbances examined by Davis and Ahijevych (2012). Even if only 10% of this DCAPE were realized (Gilmore and Wicker 1998), it would support 17 m s^{-1} downdrafts.

Strong convective downdrafts indicated by the microburst index and the large DCAPE can only be realized if deep convection is excited. The sondes in Fig. 5 exhibited a mean pseudoadiabatic CAPE of 2076 J kg^{-1}. Molinari et al. (2012) noted that adding entrainment to the CAPE calculation has an enormous impact, especially in the presence of such dry air. Estimates with 10% km^{-1} entrainment, water loading, and fusion reduced mean CAPE to 199 J kg^{-1}, which is still sufficient to produce 20 m s^{-1} updrafts. As a result, the potential for deep convection was supported in TS Edouard even after accounting for the dry midlevel air. However, these soundings also contained mean convective inhibition (CIN) of 36 J kg^{-1}. For CAPE to be realized, an updraft of 8.5 m s^{-1} would be required. This provides a reason why deep convection was not widespread in the storm. It occurred only in the downshear left quadrant, where shear-induced forcing was likely to support persistent upward motion (e.g., Reasor and Eastin 2012).

Figure 5 supports the potential for convective downdrafts in the core of TS Edouard, but soundings directly

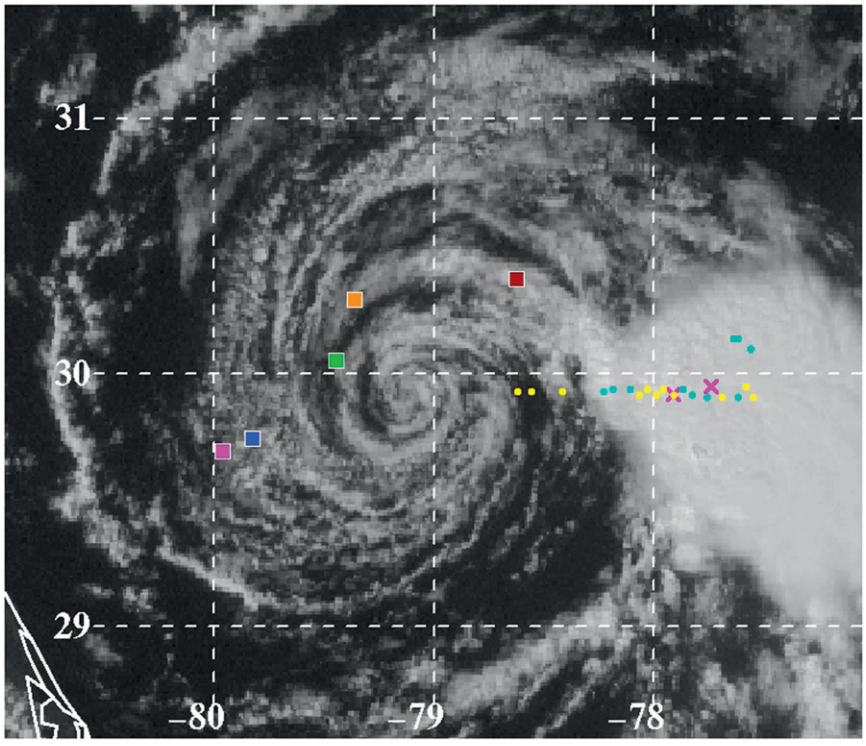

FIG. 6. Locations of G-IV sondes used in Fig. 5 (large filled colored squares), and locations of dropsondes released by two P-3 aircraft (magenta ×s) at 1851 (closer to the center) and 1854 UTC. Each location is plotted with respect to the storm center on the 1845 UTC 3 Sep visible satellite image. The small colored circles represent locations of updrafts (yellow) and downdrafts (cyan) having magnitude >0.5 m s^{-1} from the P-3 flight-level data.

displaying evidence of downdrafts were not available. Figure 6 shows the locations of two additional dropsondes (magenta ×s) released 125 km east of the center by P-3 aircraft. Although these were not in the vicinity of the earlier core convective outbreak, they will provide evidence of the nature of downdrafts in the storm. These adjacent dropsondes were released 3 min and 25 km apart by two aircraft at slightly different levels. Also shown in Fig. 6 are the locations of flight-level updrafts (filled yellow circles) and downdrafts (cyan circles) with magnitudes greater than 0.5 m s^{-1}. As noted earlier, these data represent a 7-km mean, so that 0.5 m s^{-1} represents a reasonably large value. Downdrafts, with a maximum value exceeding 4.5 m s^{-1}, existed over about a 20-km-wide zone between the two dropsondes. They were surrounded by comparable regions of updrafts. Based on the accompanying satellite image, these updrafts and downdrafts existed within strong local convection.

Figure 7a shows the vertical structure of θ_e for the two P-3 dropsondes. The 1851 UTC sonde (solid) was released about 25 km closer to the center than the 1854 UTC sounding (dashed). The former sounding exhibited θ_e 12 K lower than the adjacent sonde at the surface, while the depth of lower θ_e air extended upward from the surface to 683-m elevation. The low surface θ_e value supports the presence of strong convective downdrafts, consistent with the evidence from Fig. 6.

This conclusion is supported by the results of Barnes et al. (1983). They showed vertical profiles of θ_e in a tropical cyclone between the 90- and 70-km radii, nearly the same radial separation as the two sondes in Fig. 7a. The vertical θ_e profiles (their Figs. 10 and 11) were nearly identical to those in Fig. 7a, with 342-K values at the surface for the sonde closer to the center, and 354 K in the outer sonde. Barnes et al. (1983) attributed this structure to low-θ_e air moving downward and inward from the convective region. Didlake and Houze (2009) found similar results in an outer rainband of Hurricane Katrina (2005). Once again the cold pool formed radially inside of the band and was associated with local convective downdrafts.

Figure 7b shows the vertical distribution of DCAPE from the two soundings in Fig. 7a. Consistent with the above reasoning, large DCAPE present in the outer sounding was largely absent in the inner sounding. This

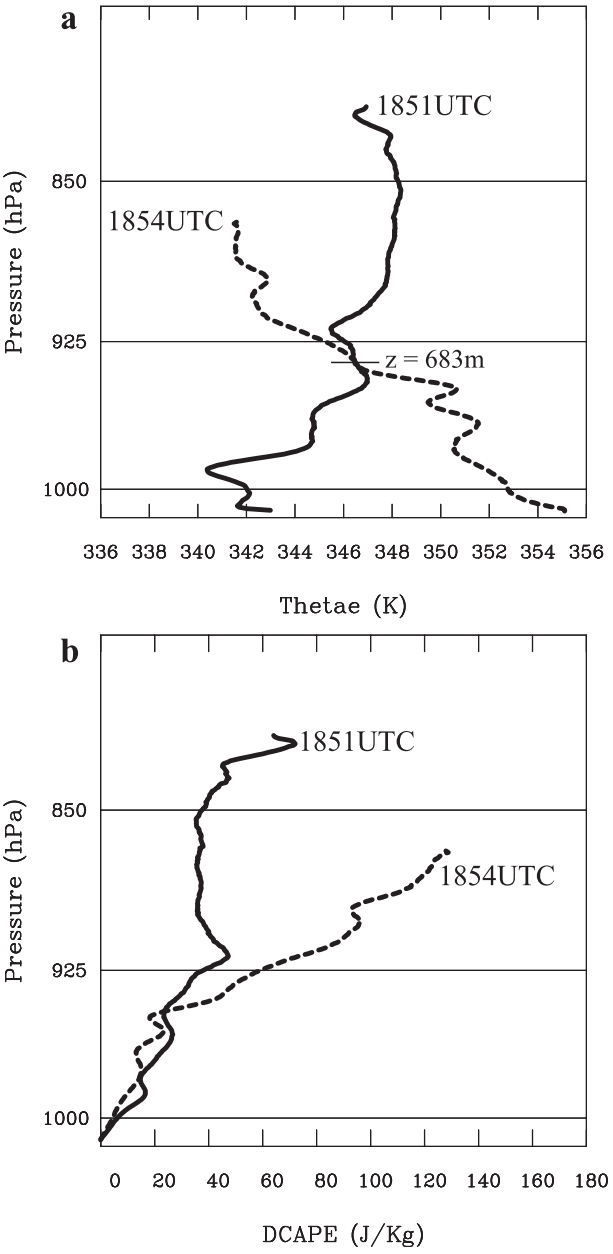

FIG. 7. (a) Comparison of the vertical profile of θ_e (K) for two dropsondes marked by magenta ×s in Fig. 6. The 1851 UTC sonde (solid) lies about 25 km closer to the center than the 1854 UTC sonde (dashed). (b) DCAPE (J kg^{-1}) for the two sondes in (a).

is strongly suggestive of consumption of DCAPE by nearby convective downdrafts.

Figure 7 indicates that low-θ_e air from convective downdrafts occurred only below 700 m. This might account for the difficulty of observing cold pools in tropical cyclones. The downdraft air in Fig. 4 might have been detectable only because U.S. Air Force reconnaissance flew below 500 m.

Direct evidence for downdrafts in Figs. 6–7 was available only 100–125 km from the center. But we believe downdrafts are also supported in the storm core, because the DCAPE in the G-IV soundings near the center (Fig. 5) was comparable to or larger than that shown in Fig. 7b. Figures 6 and 7 support the conclusion that convective downdrafts in the storm core were responsible for the cessation of convection and the subsequent weakening of the storm.

4. Discussion

Tropical Storm Edouard experienced multiple convective outbreaks in the storm core in the presence of 11–15 m s^{-1} ambient vertical wind shear, followed by extended periods without deep convection. One such sequence was studied in detail using U.S. Air Force reconnaissance data within the boundary layer. The moist entropy field (represented by θ_e) showed lower values within the convection left of shear than in regions with little lightning right of shear. Nearby soundings supported the potential for convective downdrafts to produce this low moist entropy air. The azimuthally averaged θ_e in the core of the storm, which Tang and Emanuel (2010) noted has a critical influence on intensity, was 4–6 K lower than after boundary layer recovery, consistent with the influence of downdrafts in the studies of Riemer et al. (2010) and Eastin et al. (2012).

The following sequence of events was observed: the strong core convective outbreak produced a local tangential wind of hurricane force in the downshear-left quadrant, just inside the area of strong convection. The simultaneous cold pool noted above led to a complete cessation of convection in the storm core for several hours. During this period, the azimuthal mean tangential velocity (not shown) decreased by 5 m s^{-1}, while the local tangential velocity maximum fell from 35 to 17 m s^{-1} (Fig. 4b). Tangential velocity evolved to a flat radial profile with little azimuthal variation, arguably as a consequence of axisymmetrization of the storm. Despite the weakening of tangential velocity, boundary layer θ_e recovered during this period, returning almost to a symmetric distribution. Convection erupted downshear only 2 h after that time.

When deep convection ceased in TS Edouard, so did the antifuel of cold downdrafts. This allowed boundary layer moist entropy to increase even as the storm was weakening. The sequence of events follows the reasoning of Emanuel (1993) in the Tropical Experiment in Mexico (TEXMEX). He described a ''gestation'' stage prior to rapid deepening that was produced when deep convection filled the boundary layer with cold downdrafts and completely suppressed new convection, but

also moistened middle layers. During the gestation period, strong surface fluxes restored the boundary layer, and the subsequent convective outbreak produced rapid development because the sounding had previously been moistened. Emanuel's (1993) gestation period lasted 14 h (Bister and Emanuel 1997), similar to the time difference in the first and last flights in Fig. 3.

In TS Edouard, the same sequence of boundary layer recovery after convection occurred, but by the time new convection was triggered, the strong vertical wind shear appears to have dried the column. Evidence for a broad midlevel dry air mass carried from upshear shows in the lack of variation in the minimum θ_e among the inner-core dropsondes in Fig. 5. It is hypothesized that the repeated outbreaks and cessation of convection in the core shown in Fig. 2 occurred as a result of the sequence of low-entropy downdrafts within core convection, boundary layer recovery, and renewed convection and convective downdrafts associated with strong ventilation by vertical wind shear. This oscillation is consistent with the numerical results of Tang and Emanuel (2012). It is argued, following Powell (1990), Emanuel (1993), Riemer et al. (2010), and Tang and Emanuel (2012), that the intensification and decay of tropical cyclones can be framed as a competition in the boundary layer between surface heat and moisture fluxes (fuel) and evaporation-driven low-entropy downdrafts (antifuel).

Acknowledgments. We thank Dr. Eric Rappin of the University of Miami for his suggestions on the role of boundary layer recovery. We appreciate insightful comments from two anonymous reviewers. We acknowledge outstanding efforts by the U.S. Air Force Reserve in their low-level flights in TS Edouard. Air Force reconnaissance data were made available from the website maintained by John Knaff of the Cooperative Institute for Research in the Atmosphere. NOAA P-3 data were obtained from the Hurricane Research Division of NOAA. Gridded analyses from the ECMWF were obtained from the National Center for Atmospheric Research, which is supported by the National Science Foundation (NSF). This work was supported by NSF Grants ATM0855718 and AGS1132576.

APPENDIX A

Influence of Flight Elevation Changes

Figure A1 below shows elevation changes along the flight tracks shown in Fig. 3. This appendix provides an estimate of tangential velocity (v_λ) and θ_e changes as a result of those elevation changes, and whether such changes might impact the interpretation of the data in Fig. 4.

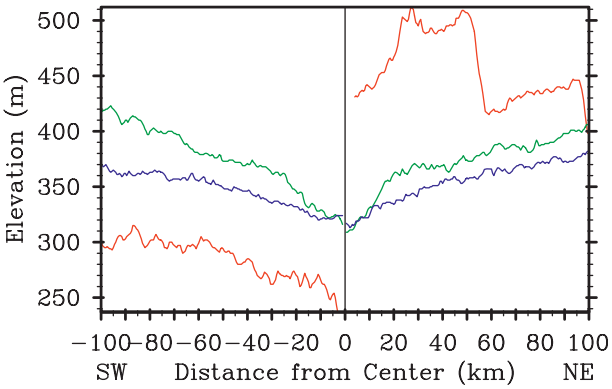

FIG. A1. Elevation of the three flights shown in Fig. 3. The black segment in Fig. 3, during which the aircraft searched for the storm center during the segments given above in red, is not displayed.

Figure 4b showed stronger v_λ left of shear during the first (red) flight than the two later flights, but the level of the first flight was about 150 m higher. Because we expect v_λ to increase with height in the boundary layer (e.g., Kepert 2006), the differences might not be as dramatic as shown. Similarly, the right-left asymmetry in v_λ during the first flight might be exaggerated by the 250-m difference in elevation. To evaluate these issues, Fig. A2 shows v_λ in the lowest km for each of the five G-IV sondes shown in Fig. 6, along with their mean. The difference in mean v_λ was <1 m s^{-1} within both the 375–500- and 250–500-m layers. Tangential velocity actually *decreased* upward over most of the 250–500-m layer. Figure A2 indicates that the differences in v_λ in Fig. 4b were not attributable to elevation differences among the flights.

The value of θ_e typically decreases with height over warm ocean. The apparent cooling by downdrafts in Fig. 4c northeast of the center, and the degree of subsequent boundary layer recovery, could be exaggerated by the 150-m elevation difference between the three northeast legs. This was addressed by examining the average decrease in θ_e in the five near-core G-IV dropsondes shown in Fig. 5b. This difference amounted to only 0.6 K in the 350–500-m layer, and 1.5 K in the 250–500-m layer. In both cases, the mean θ_e difference is much less than the observed θ_e differences in Fig. 4c. In addition, the 250–500-m θ_e difference actually reversed sign in regions near convection, presumably as a result of downdrafts, as seen in the "downdraft" profile in Fig. 7a. Because convection was occurring at the time the aircraft was at 500 m, the actual downdraft lowering of θ_e could be even larger than shown. As a result, the elevation

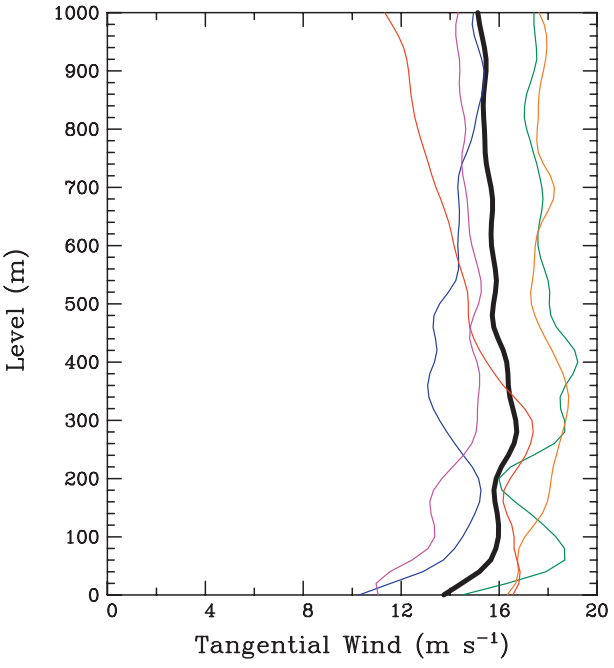

FIG. A2. Vertical variation of tangential velocity in the lowest km from the five G-IV sondes shown in Fig. 6. The heavy black line represents the mean.

changes of the aircraft likely had no impact on the identification of downdrafts and boundary layer recovery.

APPENDIX B

Flight-Level Changes in θ_e as a Result of Surface Fluxes

We wish to calculate an estimate of the time rate of change of θ_e at the levels of the U.S. Air Force reconnaissance flights as a result of sensible and latent heat fluxes from the ocean surface, in order to show that the observed changes in θ_e could be attributable to surface fluxes. We assume bulk aerodynamic formulas for surface sensible and latent heat fluxes:

$$(F_H)_0 = \rho c_p c_k |\mathbf{v}_0|(T_{\text{ocean}} - T_{\text{air}}), \tag{B1}$$

$$(F_q)_0 = \rho L c_k |\mathbf{v}_0|[q_s(T_{\text{ocean}}) - q], \tag{B2}$$

where $|\mathbf{v}_0|$ is surface wind speed, c_k represents a general enthalpy flux coefficient, and q is specific humidity. Based on recent research (L. Shay 2012, personal communication), we assume c_k is 70% of the drag coefficient c_d, which will be defined using Deacon's formula. The latter is sufficiently accurate for the tropical storm force wind speeds in TS Edouard. The following values will be used:

$\rho = 1.2$ kg m^{-3},
$|\mathbf{v}_0| = 15$ m s^{-1}, based on Fig. 4b,
$c_k = 0.7(1.85 \times 10^{-3}) = 1.3 \times 10^{-3}$,
$T_{\text{ocean}} = 29$°C (Table 1),
$T_{\text{air}} = 27$°C,
$q = 0.9q_s(T_{\text{air}})$,
$c_p = 1006$ J kg^{-1} K^{-1}, and
$L = 2.5 \times 10^6$ J kg^{-1}.

The c_k value is consistent with those of Bell et al. (2012) and Zhang et al. (2008). The assumed 2°C air–sea temperature difference might be a conservative estimate, based on surface data from the two P-3 soundings used for Fig. 7a. Those were taken over 28.5°C water, and the air–sea temperature differences were 2.5° and 4.5°C for the 1854 and 1851 UTC soundings, respectively. The corresponding surface relative humidity values were 91.6% and 87%, consistent with the 90% value assumed here.

Using the values above gives surface sensible and latent heat fluxes of 47 and 298 W m^{-2}, respectively. Adjusting for differing wind speeds, these values and their ratio are comparable to estimates in the literature (e.g., Cione et al. 2000; Shay and Uhlhorn 2008; Liu et al. 2011; Bell et al. 2012).

To evaluate the role of these fluxes at flight level (which varied from 250 to 500 m), we require a vertical profile of fluxes, which is not available from the flight data. As a result, we will make the simplest assumption: that fluxes vary linearly with height from their value at the surface to zero at the top of the boundary layer, taken to be at 1-km elevation. Then θ and q changes at any level within the boundary layer produced by surface sensible and latent heat fluxes are given by

$$\frac{d\theta}{dt} = \frac{\theta}{c_p T}\left(-\frac{1}{\rho}\frac{\partial F_H}{\partial z}\right) = \frac{\theta}{c_p T}\left(\frac{F_{H_0}}{\rho \Delta z}\right), \tag{B3}$$

$$\frac{dq}{dt} = -\frac{1}{\rho L}\frac{\partial F_q}{\partial z} = \frac{F_{q_0}}{\rho L \Delta z}, \tag{B4}$$

where F_{H_0} and F_{q_0} are given by (B1) and (B2), respectively, and $\Delta z = 1$ km. Substituting the values above gives a θ change of 1.68 K (12 h)$^{-1}$ and a q change of 4.29 g kg^{-1} (12 h)$^{-1}$. Because the percentage difference in q far exceeds that in θ, it will have the dominant influence on the increase of θ_e.

To determine boundary layer θ_e changes from these fluxes, we begin by defining θ_e:

$$\theta_e = \theta \exp\left(\frac{Lq}{c_p T_{\text{LCL}}}\right), \tag{B5}$$

where T_{LCL} represents the lifting condensation level temperature. Logarithmic differentiation gives

$$\frac{d\theta_e}{dt} = \frac{\theta_e}{\theta}\frac{d\theta}{dt} + \frac{\theta_e L}{c_p T_{LCL}}\frac{dq}{dt}. \quad \text{(B6)}$$

Changes in T_{LCL} were neglected in (B6) because sensible and latent heat fluxes have opposing impacts on LCL height, and thus on LCL temperature. We define θ_e, θ, and T_{LCL} to be 350, 300, and 295 K, respectively, noting that these could vary by a few degrees without significantly impacting the calculation. Substituting from (B1)–(B4) into (B6) gives a θ_e change of 15 K $(12\ \text{h})^{-1}$. That is larger than the observed downshear increase in θ_e, suggesting that surface enthalpy fluxes were sufficient to produce the observed boundary layer recovery. The upshear increase in θ_e was less than half that downshear, consistent with smaller air–sea temperature differences where downdrafts were much less active.

Many assumptions here could be changed. Winds at 10-m height are likely weaker than at flight level. Also, fluxes decrease more rapidly with height very near the surface than higher in the boundary layer. Assuming a linear variation through the boundary layer might overestimate them at the 250–500-m elevation of data in this study. Conversely, the boundary layer thickness in the storm core is likely less than 1 km (Zhang et al. 2011), which would enhance flux convergence and thus warming and moistening. More importantly, based on the values noted above from Fig. 5, the air–sea temperature difference could be 50% larger, and that alone would increase the total enthalpy flux by more than 50%. Finally, Molinari et al. (2012) found that mean relative humidity at the surface in the hurricane core was about 85%, not 90% assumed here, and that would add an additional 30% to the enthalpy flux. Although the calculations in this appendix represent only back-of-the-envelope estimates, they show that attributing the observed θ_e increases in Fig. 4c to boundary layer recovery from surface fluxes is a reasonable conclusion.

REFERENCES

Atkins, N. T., and R. M. Wakimoto, 1991: Wet microburst activity over the southeastern United States: Implications for forecasting. *Wea. Forecasting,* **6,** 470–482.

Barnes, G. M., E. J. Zipser, D. Jorgensen, and F. Marks Jr., 1983: Mesoscale and convective structure of a hurricane rainband. *J. Atmos. Sci.,* **40,** 2125–2137.

Bell, M. M., M. T. Montgomery, and K. A. Emanuel, 2012: Air–sea enthalpy and momentum exchange at major hurricane wind speeds observed during CBLAST. *J. Atmos. Sci.,* **69,** 3197–3222.

Bister, M., and K. A. Emanuel, 1997: The genesis of Hurricane Guillermo: TEXMEX analyses and a modeling study. *Mon. Wea. Rev.,* **125,** 2662–2682.

Cione, J. J., P. G. Black, and S. H. Houston, 2000: Surface observations in the hurricane environment. *Mon. Wea. Rev.,* **128,** 1550–1561.

Corbosiero, K. L., and J. Molinari, 2002: The effects of vertical wind shear on the distribution of convection in tropical cyclones. *Mon. Wea. Rev.,* **130,** 2110–2123.

Cram, T. A., J. Persing, M. T. Montgomery, and S. A. Braun, 2007: A Lagrangian trajectory view on transport and mixing processes between the eye, eyewall, and environment using a high-resolution simulation of Hurricane Bonnie (1998). *J. Atmos. Sci.,* **64,** 1835–1856.

Cummins, K. L., and M. J. Murphy, 2009: An overview of lightning locating systems: History, technique, and data uses, with an in-depth look at the U.S. NLDN. *IEEE Trans. Electromag. Compat.,* **51,** 499–518.

Davis, C. A., and D. A. Ahijevych, 2012: Mesoscale structural evolution of three tropical weather systems observed during PREDICT. *J. Atmos. Sci.,* **69,** 1284–1305.

DeMaria, M., 1996: The effect of vertical shear on tropical cyclone intensity change. *J. Atmos. Sci.,* **53,** 2076–2087.

Didlake, A. C., and R. A. Houze Jr., 2009: Convective-scale downdrafts in the principal rainband of Hurricane Katrina (2005). *Mon. Wea. Rev.,* **137,** 3269–3293.

Eastin, M. D., P. G. Black, and W. M. Gray, 2002: Flight-level thermodynamic instrument wetting errors in hurricanes. Part I: Observations. *Mon. Wea. Rev.,* **130,** 825–841.

——, W. M. Gray, and P. G. Black, 2005: Buoyancy of convective vertical motions in the inner core of intense hurricanes. Part II: Case studies. *Mon. Wea. Rev.,* **133,** 209–227.

——, T. L. Gardner, M. C. Link, and K. C. Smith, 2012: Surface cold pools in the outer rainbands of Tropical Storm Hanna (2008) near landfall. *Mon. Wea. Rev.,* **140,** 471–491.

Emanuel, K. A., 1986: An air-sea interaction theory for tropical cyclones. Part I: Steady-state maintenance. *J. Atmos. Sci.,* **43,** 585–605.

——, 1993: The physics of tropical cyclogenesis over the eastern Pacific. *Tropical Cyclone Disasters,* J. Lighthill et al., Eds., Peking University Press, 136–142.

——, 1994: *Atmospheric Convection*. Oxford University Press, 580 pp.

Frank, J. D., 2008: Evolution of a tropical storm in strong vertical wind shear. M.S. thesis, Department of Atmospheric and Environmental Sciences, University at Albany, State University of New York, Albany, NY, 163 pp.

Gilmore, M. S., and L. J. Wicker, 1998: The influence of midtropospheric dryness on supercell morphology and evolution. *Mon. Wea. Rev.,* **126,** 1943–1958.

Kepert, J. D., 2006: Observed boundary layer wind structure and balance in the hurricane core. Part I: Hurricane Georges. *J. Atmos. Sci.,* **63,** 2169–2193.

Liu, J., J. A. Curry, C. A. Clayson, and M. A. Bourassa, 2011: High-resolution satellite surface latent heat fluxes in North Atlantic hurricanes. *Mon. Wea. Rev.,* **139,** 2735–2747.

Molinari, J., and D. Vollaro, 2010: Rapid intensification of a sheared tropical storm. *Mon. Wea. Rev.,* **138,** 3869–3885.

——, D. M. Romps, D. Vollaro, and L. Nguyen, 2012: CAPE in tropical cyclones. *J. Atmos. Sci.,* **69,** 2452–2463.

Möller, J. D., and M. T. Montgomery, 2000: Tropical cyclone evolution via potential vorticity anomalies in a three-dimensional balance model. *J. Atmos. Sci.,* **57,** 3366–3387.

Montgomery, M. T., and R. J. Kallenbach, 1997: A theory for vortex Rossby waves and its application to spiral bands and intensity changes in hurricanes. *Quart. J. Roy. Meteor. Soc.,* **123,** 435–465.

Nolan, D. S., 2011: Evaluating environmental favorableness for tropical cyclone development with the method of point-downscaling. *J. Adv. Model. Earth Syst.,* **3,** M08001, doi:10.1029/2011MS000063.

——, and M. G. McGauley, 2012: Tropical cyclogenesis in wind shear: Climatological relationships and physical processes. *Cyclones: Formation, Triggers, and Control,* K. Oouchi and H. Fudeyasu, Eds., Nova Science Publishers, 1–36.

Powell, M. D., 1990: Boundary layer structure and dynamics in outer hurricane rainbands. Part II: Downdraft modification and mixed layer recovery. *Mon. Wea. Rev.,* **118,** 918–938.

Reasor, P. D., and M. D. Eastin, 2012: Rapidly intensifying Hurricane Guillermo (1997). Part II: Resilience in shear. *Mon. Wea. Rev.,* **140,** 425–444.

Riemer, M., and M. T. Montgomery, 2011: Simple kinematic models for the environmental interaction of tropical cyclones in vertical wind shear. *Atmos. Chem. Phys.,* **11,** 9395–9414.

——, ——, and M. E. Nicholls, 2010: A new paradigm for intensity modification of tropical cyclones: Thermodynamics impact of vertical wind shear on the inflow layer. *Atmos. Chem. Phys.,* **10,** 3163–3188.

Shay, L. K., and E. W. Uhlhorn, 2008: Loop current response to Hurricanes Isidore and Lili. *Mon. Wea. Rev.,* **136,** 3248–3274.

Shelton, K., and J. Molinari, 2009: Life of a six-hour hurricane. *Mon. Wea. Rev.,* **137,** 51–67.

Smith, R. K., and M. T. Montgomery, 2011: Observations of the convective environment in developing and non-developing tropical disturbances. *Quart. J. Roy. Meteor. Soc.,* **137,** 1–18.

Tang, B., and K. Emanuel, 2010: Midlevel ventilation's constraint on tropical cyclone intensity. *J. Atmos. Sci.,* **67,** 1817–1830.

——, and ——, 2012: Sensitivity of tropical cyclone intensity to ventilation in an axisymmetric model. *J. Atmos. Sci.,* **69,** 2394–2413.

Wheeler, M. M., and W. P. Roeder, 1996: Forecasting wet microburst on the central Florida Atlantic coast in support of the United States Space Program. Preprints, *18th Conf. on Severe Local Storms,* San Francisco, CA, Amer. Meteor. Soc., P7.4.

Willoughby, H. E., F. D. Marks Jr., and R. J. Feinberg, 1984: Stationary and moving convective bands in hurricanes. *J. Atmos. Sci.,* **41,** 3189–3211.

Zhang, J. A., P. G. Black, J. R. French, and W. M. Drennan, 2008: First direct measurements of enthalpy flux in the hurricane boundary layer: The CBLAST results. *Geophys. Res. Lett.,* **35,** L14813, doi:10.1029/2008GL034374.

——, R. F. Rogers, D. S. Nolan, and F. D. Marks Jr., 2011: On the characteristic height scales of the hurricane boundary layer. *Mon. Wea. Rev.,* **139,** 2523–2535.

Zipser, E. J., 1977: Mesoscale and convective-scale downdrafts as distinct components of squall-line circulation. *Mon. Wea. Rev.,* **105,** 1568–1589.